JOURNAL OF Applied Polymer SCIENCE

Electrical conduction in plasma polymerized thin films of γ-terpinene

Jakaria Ahmad,[1] Kateryna Bazaka,[1]* Krasimir Vasilev,[2] Mohan V. Jacob[1]

[1]Electronic Materials Research Laboratory, College of Science, Technology and Engineering, James Cook University, Townsville 4811, Australia

[2]Division of Information Technology, Engineering and the Environment, Mawson Institute, University of South Australia, Mawson Lakes, Adelaide, Australia

*Present address: School of Chemistry, Physics, and Mechanical Engineering, Queensland University of Technology, Brisbane, QLD 4000, Australia

Correspondence to: M. V. Jacob (E-mail: mohan.jacob@jcu.edu.au)

ABSTRACT: Plasma polymerized γ-terpinene (pp−GT) thin films are fabricated using RF plasma polymerization. MIM structures are fabricated and using the capacitive structures dielectric properties of the material is studied. The dielectric constant values are found to be in good agreement with those determined from ellipsometric data. At a frequency of 100 kHz, the dielectric constant varies with RF deposition power, from 3.69 (10 W) to 3.24 (75 W). The current density–voltage ($J-V$) characteristics of pp–GT thin films are investigated as a function of RF deposition power at room temperature to determine the resistivity and DC conduction mechanism of the films. At higher applied voltage region, Schottky conduction is the dominant DC conduction mechanism. The capacitance and the loss tangent are found to be frequency dependent. The conductivity of the pp−GT thin films is found to decrease from 1.39×10^{-12} S/cm (10 W) to 1.02×10^{-13} S/cm (75 W) and attributed to the change in the chemical composition and structure of the polymer. The breakdown field for pp–GT thin films increases from 1.48 MV/cm (10 W) to 2 MV/cm (75 W). A single broad relaxation peak is observed indicating the contribution of multiple relaxations to the dielectric response for temperature dependent J−V. The distribution of these relaxation times is determined through regularization methods. © 2015 Wiley Periodicals, Inc. J. Appl. Polym. Sci. **2015**, *132*, 42318.

KEYWORDS: biopolymers and renewable polymers; dielectric properties; properties and characterization

Received 8 January 2015; accepted 6 April 2015

DOI: 10.1002/app.42318

INTRODUCTION

Plasma polymerization or plasma–enhanced chemical vapor deposition (PECVD)[1] is a promising modern technique for direct polymer thin films deposition of varying thickness on various substrates from almost any organic vapor.[2,3] The properties of the polymers obtained by this method are of high quality, different, and in contradistinction to the conventional polymerization methods.[4,5] By employing this technique it is possible to deposit polymer films that are generally homogeneous, adherent, pinhole free, chemically inert, adhesive, and thermally stable.[4,6,7] The properties of the thin films can also be altered by varying the deposition parameters like deposition power, pressure, monomer flow rate, and deposition time.[2] These films have therefore been extensively investigated in the recent past due to their potential applications in electronics and optoelectronics.[8–12] They can be used as insulating, dielectric, and functional layers for electronic functional elements in thin film transistors, diodes, switching elements, photovoltaic (PV) devices, capacitors, etc.[11,13,14] However, plasma polymerization usually yields polymer of highly cross-linked, highly branched and highly insulating materials and applications of these polymers are therefore mostly suited for the field of dielectric films.[15,16]

In organic thin film transistors (OTFTs) a gate insulating material is generally used. As an example polymethyl-methacrylate-cog-lyciclyl-methacrylate (PMMA-GMA) is employed as the gate insulator with dielectric constant (k) of ~3.9.[17] Another polymeric material has been developed from pyrrole by radio frequency (RF) PECVD with $k \cong 3.8$.[16] However, there are several drawbacks in the devices with these high–k material including high leakage current and hysteresis.[17] It is also important to decrease the thickness of the gate dielectric. In conventional metal−oxide−semiconductor (MOS), for 2.0 μm to 0.25 μm nodes, tetraethyl orthosilicate (TEOS) with a dielectric constant k of < 4 is typically used as the interlayer dielectrics (ILD) material.[8] Fluorinated silicon oxide (FSO) offers a lower dielectric

constant of < 3.5, due to lower polarizability of Si—F bonds compared with Si—O bonds. The lowest dielectric constant values achievable by FSO are in the range 3.2−3.7, which are not sufficiently low for complementary MOS technologies of 0.13 μm and below.[9] A number of reliability concerns also accompany the use of FSO as an ILD.[18] Even lower values of k have been achieved by introducing organic groups, such as CH_3, and Si—H terminals into the silica network yielding organosilica glasses (OSG) with $k \sim 2.7-3.0$. However, to ensure process compatibility and high device reliability, materials need to meet some electrical requirements as well as suitable dielectric behavior.[19]

Another important application for organic thin films is organic photovoltaics (OPV). OPV technology is economically competitive and it virtues collective advantages such as manufacturing adaptability, low-cost processing and a lightweight, flexible device end product, reel-to-reel processing on low cost substrates, with numerous printing techniques, namely screen, inkjet, offset or flexo printing, already available.[20,21] However, the OPV technology is yet to reach a desirable level of performance, which would render it suitable for wide commercial use.[11] Present power conversion efficiency (PCE) and operational stability of OPV are considerably lower than those offered by Si technology. Significant research efforts have been devoted to development of materials, designs, and structures to improve PCE of OPV, with a recent report of 12% for an organic cell. Although this value falls short of ∼25% PCE level offered by Si PV cells, it may well be sufficient for a feasible commercial proposition when substantially less expensive production budget for OPV is considered. Long-term operation stability of OPV, however, is far below what would be considered acceptable for a commercial product, with the replacement costs negating the cost savings from inexpensive manufacturing. Currently, the acceptable lifetime of an inorganic solar cell is 20–25 years,[22] well beyond the lifetime achievable by the most advanced organic solar cells available. Such profound discrepancy in device life expectancy between inorganic and organic PV cells stems from relatively high susceptibility of organic materials to water vapor and oxygen, which lead to reduced reliability and lifetime of organic devices under normal environmental conditions.[11,23] Encapsulation with high barrier performance materials and structures is one of the key ways to address these issues and improve device lifetime.[24–27]

Thin film encapsulation is a critical technology required for the application and commercialization of OPVs.[11] For effective encapsulation, the materials have to meet the requirements of good processability, high optical transmission, high dielectric constant, low water absorptivity and permeability, high resistance to ultra-violet (UV) degradation and thermal oxidation, good adhesion, mechanical strength, and chemical inertness.[11] However, the materials currently available cannot yet satisfy these aforementioned requirements. Adhesion strength of ethylene vinyl acetate (EVA), for example, is affected by the processing conditions, damp heat, and exposure time.[28] The deposition of the SiO_x and SiN_x encapsulation structure causes plasma damage on the devices owing to the high sensitivity of the organic films to radiation, charging and heating.[29,30] Al_2O_3 has a slow deposition rate compared to PECVD-based methods that makes it more difficult to use in low-cost mass manufacturing processes.[11] New materials are needed which will satisfy the encapsulation requirements and achieve the reliability and lifetime required.

Polyterpenol[31] and poly–linalyl acetate[32] are two new materials fabricated from nonsynthetic environmentally sustainable source that were investigated to be used as insulating material in organic electronics. They were demonstrated to be promising insulating materials. 1-isopropyl-4-methyl-1,4-cyclohexadiene comes from the same monomer family as terpenol–4–ol and linalyl acetate and has therefore been used in this study to synthesize an organic polymer by RF PECVD. The precursor, also known as γ-terpinene, is a natural, minimally processed plant-derived source, and is considered as an environmentally friendly alternative to highly purified monomers typically used for fabrication of electronic materials. The fabricated polymer (pp–GT) thin films are transparent to the optical wavelengths, with an energy gap of 3.1 eV indicative of an insulating material.[2] In terms of surface morphology, the films are smooth (average roughness around 0.3 nm), uniform, defect free, and show high adhesion to a variety of substrates.[2] The pp−GT are stable when in contact with many types of common solvents. Moderately hydrophobic, the films are completely wetted by chloroform and chlorobenzene, the solvent commonly used in deposition of organic semiconducting layers.[33] Since the performance of an organic device relies on the charge carrier injection and transport in the active material, adequate understanding of the nature of the carrier transport within the polymer thin films is significant for microelectronic and optoelectronic applications. As such, with potential application as an encapsulating and ILD material, this work investigates the electrical properties of pp−GT films, specifically the dielectric constant, conductivity and breakdown field. These properties were investigated as a function of deposition conditions, input RF energy used for fabrication, and frequency and temperature dependence on the structural and chemical properties of pp–GT material.

EXPERIMENTAL

Sample Preparation

Thin film samples were deposited on high quality glass microscope slides inside a custom made, cylindrical RF polymerization chamber, 0.75 m in length with an inner diameter of 0.055 m (approximate volume of 0.018 cm^3). Extran and ultrasonic bath of distilled water was used to thoroughly clean the substrates. These were also rinsed with isopropanol and air dried prior to deposition. Using the procedure outlined in,[34] plasma polymer films of ∼800 nm thickness were fabricated from γ-terpinene monomer at various RF deposition power levels (10, 25, 50, and 75 W). Time of deposition was varied to obtain films of desired thickness.

For J–V measurements, three-layered sandwich MIM structures (*Al*/pp–GT thin film/*Al*) were deposited onto thoroughly cleaned glass substrates. Using a custom made shadow mask, devices were prepared by first depositing bottom *Al* electrode using thermal evaporation at a pressure of 10^{-6} Torr. The pp−GT thin films were then fabricated using RF plasma polymerization. Finally, top electrodes were deposited using thermal evaporation technique and the electrical contact was made by

Table I. Dielectric Properties of pp–GT Thin Films Determined from Capacitive Measurements

	ε_r			
Sample	100 Hz	1 KHz	10 KHz	100 KHz
10 W	3.98	3.89	3.81	3.69
25 W	3.84	3.76	3.66	3.57
50 W	3.72	3.63	2.55	3.44
75 W	3.41	3.38	3.32	3.24

the conductive silver epoxy (CW2400). The bottom and top *Al* electrodes were rectangular in shape with an effective area of $\sim 3 \times 10^{-5}$ m^2.

Measurements

The thickness measurements of the pp–GT thin films were performed by M-2000, J. A. Woollam. variable angle spectroscopic ellipsometer (VASE). Hioki 3552-50 LCR meter was used to analyze the dielectric function between frequencies of 10 Hz–100 kHz. The impedance z, capacitance C, phase angle θ and dielectric loss tan δ were measured with no applied DC bias. From these values together with the device geometry, real, and imaginary parts of the dielectric constant ε_r and $\varepsilon_r^{'}$ of the thin films were determined from the following relations:

$$\varepsilon_r = \frac{dC}{A\varepsilon_0} \quad (1)$$

$$\varepsilon_r^{'} = \varepsilon_r \tan\delta \quad (2)$$

where d is the thickness of the film, A is the cross section area, and ε_o is the permittivity of free space.

Temperature measurements were performed using the same measurement device by placing the samples on a temperature-controlled hotplate (323 K, 333 K, 343 K, and 348 K). The sample was left on the hotplate for 10 min at each temperature to ensure uniform heating, and the temperature of the sample was confirmed via a digital thermocouple prior to measurement of the dielectric function.

Dielectric breakdown measurements were performed on the MIM structures using a Keithley 2636A source meter. A staircase function swept the voltage and current was measured until a sudden increase in current occurred. The point at which the meter indicated current limiting was set at 100 μA for all devices so that the short circuit current could be clearly ascertained from the current–density voltage (J–V) plot.

RESULTS AND DISCUSSION

Dielectric Properties

Dielectric polarization and relaxation effects govern the behavior of dielectric properties of polymeric materials as a function of frequency. The dielectric relaxation mechanisms can be grouped into three classes, viz. α, β, and γ relaxations in order of decreasing temperature.[35,36] α relaxation is a high temperature process that may involve crystalline regions and is usually related to the main chain motions. Its intensity increases with the degree of crystallinity.[37] The β relaxation process is related to the movement of the side group chains or branches of the polymer and it related to the amorphous regions. The γ-process is related to the local intermolecular relaxation at a temperature below T_g.[37] Since the measurement temperature in this section of the study is maintained constant, the identification of the different relaxation mechanisms (α, β, γ) becomes difficult without studies involving temperature.

Results of the dielectric constants of the pp–GT thin films are summarized in Table I. Representative curves of the dielectric function of pp–GT thin films at various power levels are also depicted in Figure 1. The experimental results indicate that the dielectric constant value decreases with increasing the RF deposition power. This is attributed to increase of carbon and decrease of oxygen content in pp–GT films with RF deposition power.[33] The initial decrease in dielectric constant at low frequencies can be traced to orientational polarizations of trapped free radicals, unpaired electron sites, oligomeric structures, and polar groups under an applied external electrical field.[38] Higher dielectric constant has also been previously reported in the low frequency region for other plasma deposited thin films, and was generally attributed to interfacial phenomena (e.g., formation of depletion regions and interfacial polarizations) at the metal/insulator junction due to inefficiency of charge transport through the interface under applied electric field.[16] Interfacial phenomena is less dominant at higher frequencies with the measured capacitance approaching the bulk, or insulator capacitance. Steadily decreasing dielectric constant is observed for all pp–GT thin films in higher frequency region. The dielectric constant is generally composed of contributions from electronic, ionic, and orientational polarizations.[32]

The pure electronic contribution to the dielectric constant was calculated from the refractive index (n) obtained in the UV/Vis region. Since the extinction coefficient (k) is normally negligible

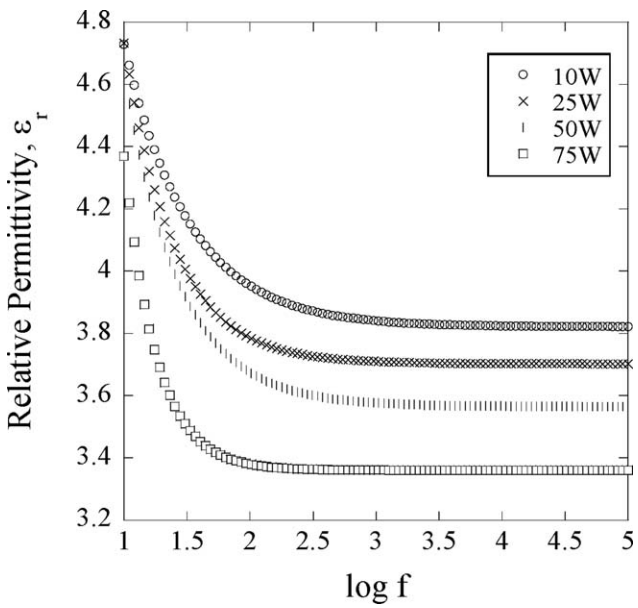

Figure 1. Frequency dependence of the dielectric function of pp–GT thin films at various power levels.

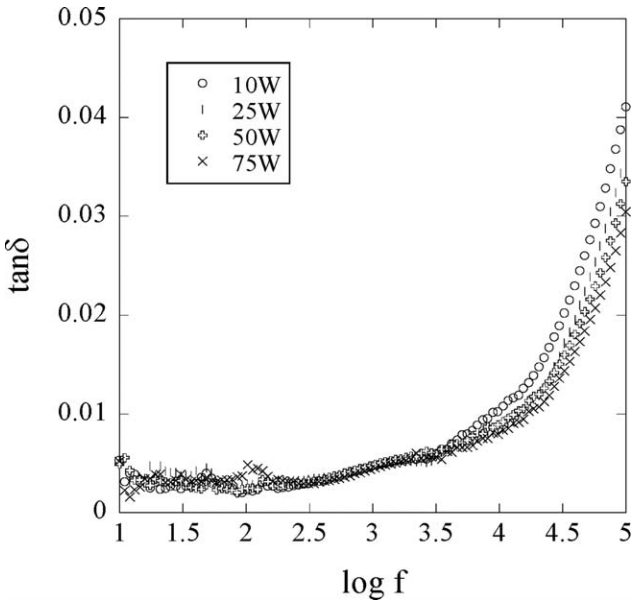

Figure 2. Dielectric losses *vs.* log f for pp–GT thin films at different RF deposition power.

in this region, the relative dielectric constant can be simply expressed as:[39]

$$\varepsilon_{\text{electronic}} = n^2 \tag{3}$$

For validating the dielectric constants of pp–GT polymer thin films, data from ellipsometric study were used. If the refractive index, n, of a sample at optical frequencies (~600 nm) is considered, the value of $\varepsilon_{\text{electronic}}$ is estimated to be 2.44. Hence, contribution from electronic phenomena is ~61.3–75.3% of the dielectric constant at frequencies greater than 10 Hz. Ionic and orientational phenomena contribute the rest in the bulk of the plasma deposited thin films. Large amount of cross–linking induced by the plasma deposition process is the reason for these low contributions, as cross–linking reduces molecular mobility and ionic polarization of molecular structures present in the bulk of the material.[40] The frequency dependence of ε_r is indicative of electronic polarization[35] due to oligomers/fragments, polar side groups, and residual free radicals effects on interfacial polarization and microscopic field distortion.

Dielectric Loss. The dielectric dissipation factor (also known as power factor or electrical loss tangent) tan δ is one of the key electrical properties of the polymer. It is defined as the ratio of an insulating material's resistance to its capacitive reactance at a specified frequency. It is always greater than 0, but usually much smaller than the dielectric constant. Loss tangent measurements are an excellent means of quality control that can yield indication of degradation or moisture pick-up. It is important in many applications such as in the insulation of cables, encapsulates for OPV and electric components, ILD, and printed wiring board materials.

The variations of the dielectric loss tangent, tan δ, with respect to frequency in pp–GT thin films at different input power levels are shown in Figure 2. It is observed that all samples show similar behavior, reaching a minimum value at ~100 Hz before beginning to increase again. Both the magnitude and characteristics of the dielectric loss values as a function of frequency are similar to other plasma deposited films.[32]

In this study, the capacitor system is assumed to comprise a frequency–independent capacitive element C' in parallel with a resistive element R, whereas both are in series with a constant low value resistance r. The measured equivalent series capacitance C_s, of the circuit is governed by:

$$C_s = C' + \frac{1}{\omega^2 R^2 C'} \tag{4}$$

This equation reveals that the measured capacitance C_s should decrease with increasing frequency. The loss tangent is given by:

$$\tan\delta = \frac{\left(1+\frac{r}{R}\right)}{\omega RC'} + \omega r C' \tag{5}$$

where ω is the angular frequency. This equation reveals that tan δ is proportional to the frequency and is not dependent on charge carrier concentrations within the material. Thus, the eq. (4) predicts a decrease in tan δ at low frequency followed by a loss minimum at:[41]

$$\omega_{\min} \approx \left(\frac{1}{rRC'^2}\right)^{1/2} \tag{6}$$

and an increase in tan δ at high frequency. Figure 2 demonstrates that in all the pp–GT thin films, initial drop is followed by an increase in tan δ values with increasing frequency. This increase is dominated by resistive losses since the mobile charges contained in the film cannot follow higher frequency electric fields. This loss of energy is associated with the degree of orientation of molecules in addition to the degree of internal friction of the polymer.[19] Since pp−GT films are strongly cross–linked, the polymer backbones have limited molecular mobility and this loss of rigidity of the polymer network facilitates the translational motion of charged impurities. The increase in tan δ with frequency can therefore be attributed to the introduction of polar impurities in the pp–GT polymers.[42]

Lower tan δ values at low frequencies in pp–GT thin films can be due to a lower electrical conductivity in them. The motion of charge carriers that contributes to the conductivity at high frequencies occurs predominantly along polymer chains.[43] Defects and inter-chain charge transport can create a barrier to the charge transport in polymers that can in turn cause a reduction in electrical conductivity. The presence of a number of polymer chain entanglements in pp–GT thin films are the probable reasons for the motion of charges in the system that caused a reduction in the electrical conductivity (hence lower tan δ values). For any electrical insulation system, a low tan δ value is always desired in the dielectric material whereas the desired permittivity of the material can be high or low depending on the end application.[44] Lower tan δ values of pp–GT thin films can therefore be suitable for use in electrical insulation systems.

Temperature Dependence of the Dielectric Constant. The capacitance of pp–GT thin films as a function of frequency is measured at different temperatures as shown in Figure 3. It is observed that the capacitance is frequency dependent at all frequencies. Similar results have been obtained and were

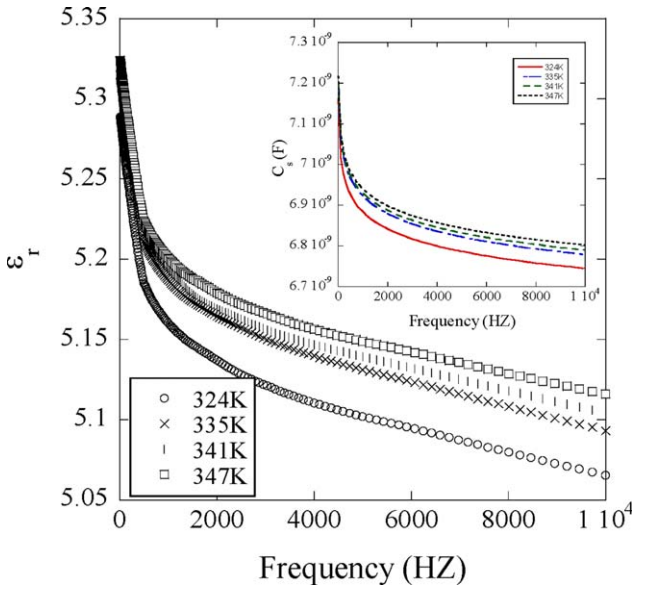

Figure 3. Real part of the dielectric function and frequency dependence of capacitance (inset) for pp–GT thin films (50W) at different temperatures. [Color figure can be viewed in the online issue, which is available at wileyonlinelibrary.com.]

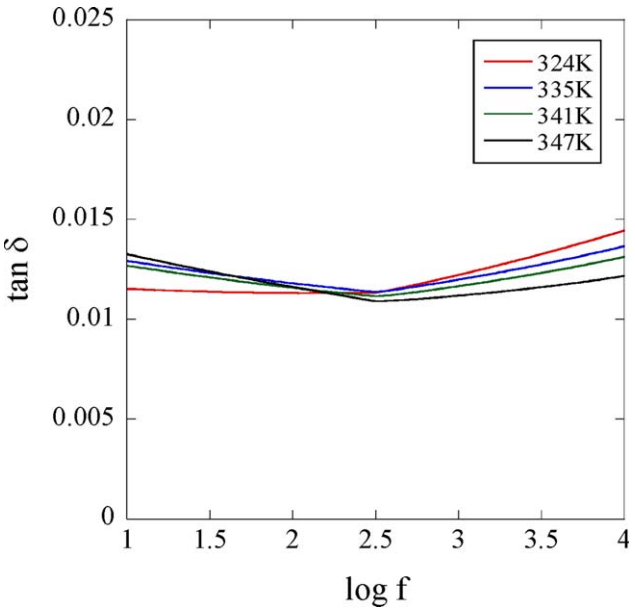

Figure 4. Frequency dependence of loss tan δ for pp–GT thin films (50W) at different temperatures. [Color figure can be viewed in the online issue, which is available at wileyonlinelibrary.com.]

adequately interpreted in terms of an equivalent circuit model.[45] According to this model the measured capacitance C_s is given by eq. (4). This equation reveals the decrease of C_s with increasing frequency and that for any given frequency, C_s will increase with increasing temperature. pp–GT thin films show the same behavior.

The dielectric constants, ε_r (eq. (1)) at different temperatures for pp–GT thin films has also been observed to decrease with increasing frequency (Figure 3). This decrease can be attributed to the fact that at low frequencies, ε_r for a polar material is due to the contribution of multi-components of polarizability, deformational, and relaxation polarization.

Figure 3 also revealed that ε_r increases with increasing temperature. This increase can be attributed to the fact that the orientational polarization is connected with the thermal motion of molecules. Dipoles cannot therefore orient themselves at low temperatures.[46] When the temperature is increased the orientation of dipoles is facilitated and this increases the value of orientational polarization, which increases ε_r.[46]

Temperature Dependence of the Dielectric Loss. The variation of tan δ with frequency at various temperatures is represented in Figure 4. The expression of tan δ (eq. (5)) predicts a decrease in tan δ with increasing frequency[45] and an increase with frequency above $\omega_{min} = 1/[C'(rR)^{1/2}]$, where the term in ω is dominant. As shown in Figure 4, the decrease of tan δ with frequency is evident as predicted for low frequency and a loss minimum is observed at ~300 Hz. After this point, tan δ started to increase with frequency.

Relaxation Time Distributions. The imaginary part of the measured dielectric function (Figure 5) reveals distinct relaxation features in the measured data at all temperatures, shifting from lower to higher frequencies as temperature increases. The width of these peaks is quite large, indicating contributions from multiple relaxation times.

The Cole–Cole plots of the real part dielectric constant (ε_r) on its imaginary part dielectric loss (ε_r') of pp–GT films at different temperatures are also shown in Figure 6 and the centers in the figures lie above the abscissa axes. This confirms that there exists a distribution of relaxation times in pp–GT films.[46] It is clear from Figure 5 also that ε_r' increases with increasing temperature. At low temperatures conduction losses (one of the three parts of relaxation phenomena) have minimum value. As the temperature increases the conductivity increases and so the

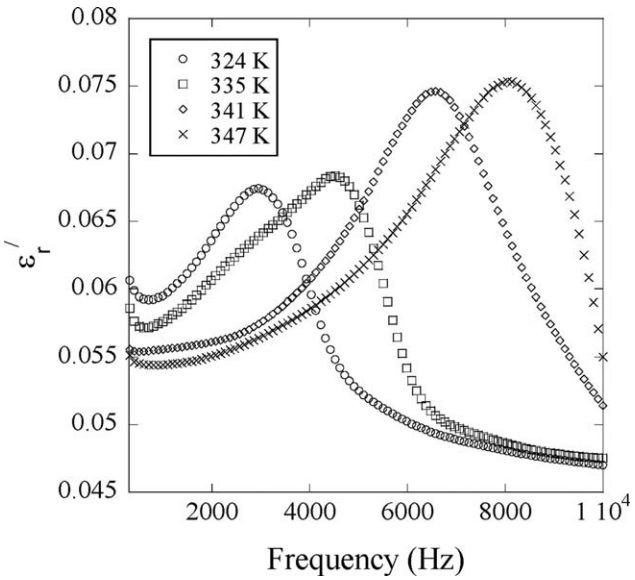

Figure 5. Imaginary part of the dielectric function measured at 324, 335, 341 and 347 K for pp–GT thin films (50W).

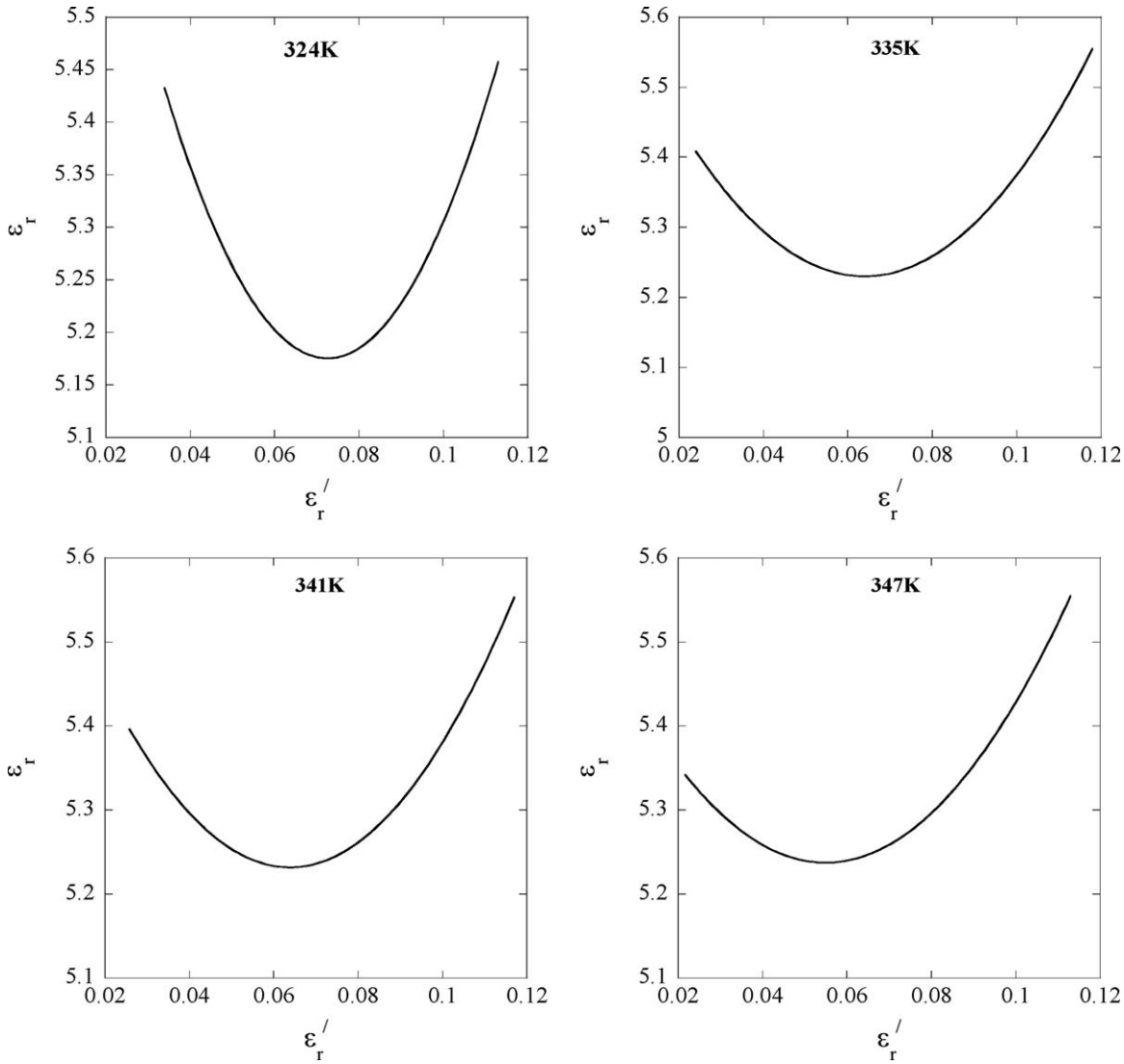

Figure 6. The variation of the real dielectric constant ε_r on its imaginary part ε_r' of pp–GT films (50W) at different temperatures for different frequencies.

conduction losses increases. This increases the value of ε_r' with increasing temperature.[46]

Figure 7 shows the approximate discrete relaxation time distributions derived from dielectric measurements at 323 K, 333 K, 343 K, and 348 K as histograms showing the relative contribution of each relaxation time to the overall dielectric function. Each of the distributions show a dominant feature of higher magnitude than any others that moved to smaller relaxation times as the temperature increased. This feature corresponded to the peak measured in the imaginary permittivity data and approximately four additional peaks contributed to the overall dielectric function. The presence of these additional peaks in the relaxation time distribution reveals information not immediately evident from the dielectric spectroscopy measurements, which indicated the possibility of presence of a single relaxation process. At 348 K, a large portion of the relaxation peak was outside the measurable frequency range of the meter. The behavior at relaxation times below the principle group characteristic to measurements at 323 K, 333 K, and 343 K was therefore not present in the sample measured at 348 K. These features demonstrate the highly fragmented, cross–linked nature of the pp–GT films.

J–V Study

Various mechanisms have been suggested for the carrier transport in polymer thin films based on the dependence of current density on voltage, temperature, and thickness. To ascertain the prevalence of a particular mechanism it is necessary to investigate the dependence of current density on the above-mentioned parameters. In this study, conduction mechanisms were investigated for pp–GT thin films by measuring standard *I–V* characteristics in the voltage range 0–200 V. For all examined devices, the measured *I–V* dependence showed low current over a wide range of applied voltage. Figure 8 shows the observed current density, *J*, of devices at room temperature with an applied voltage between 0 V and 200 V. Independent of pp–GT thin film deposition conditions, the $J-V$ curves have approximately the same shape,

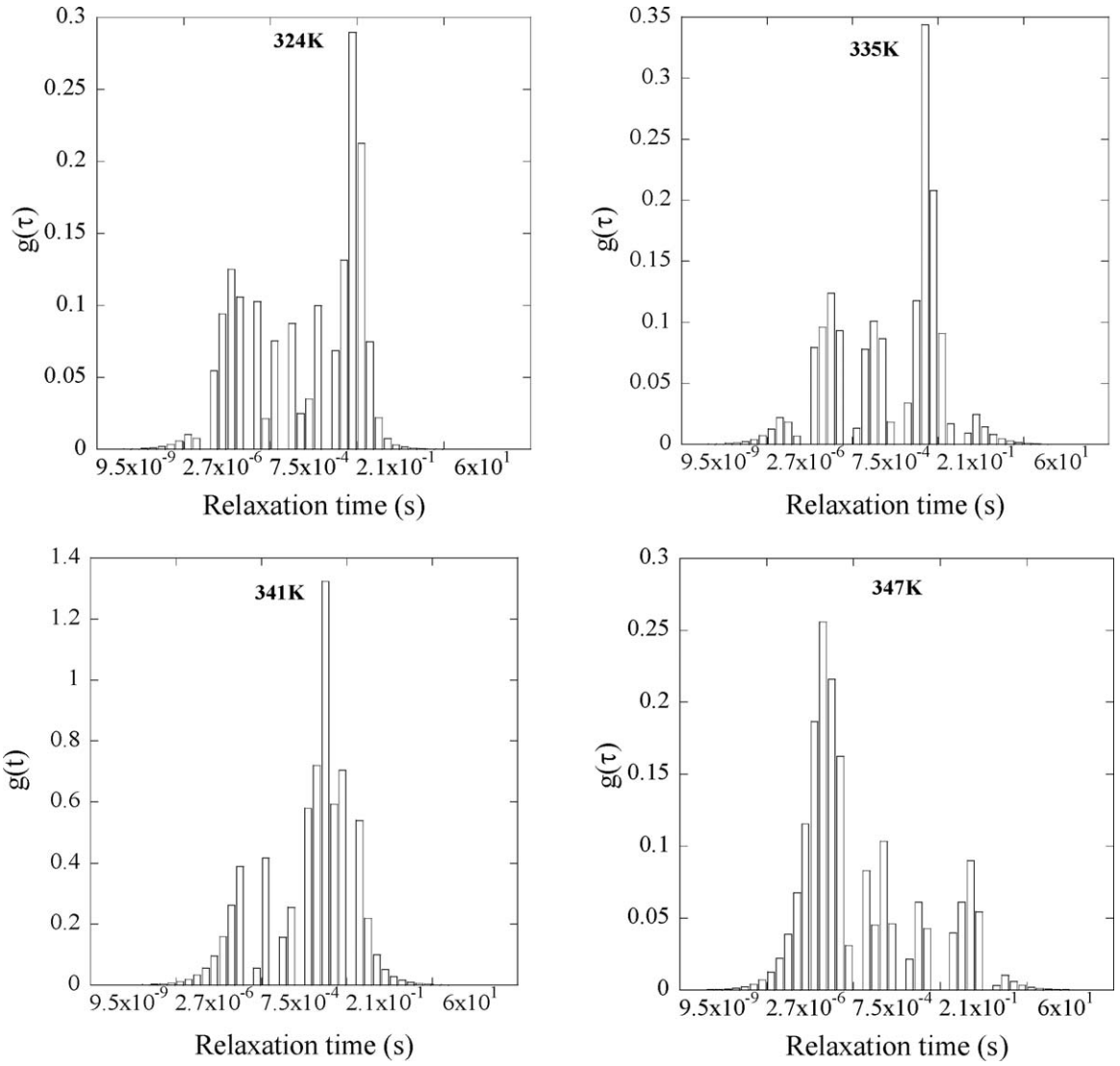

Figure 7. Distribution of relaxation times evaluated from dielectric spectra at 323 K, 333 K, 343 K and 348 K for pp–GT thin films (50W)

having two sections of different slope in the low and high voltage regions that implies two different conduction processes.

In the low field region, the $J-V$ characteristic can be described by a power law relation, where $J \propto V^m$, m being the power law index.[47] In this region, the value of m for all pp–GT thin films lies within the range of $0.5 < m < 0.7$ and the current density J can be considered to exhibit an approximately ohmic dependence with the applied voltage, V.[47] Ohmic conduction describes injection of carriers through the bulk of the material, limited only by the device geometry and number of carriers available for transport and the material mobility. In this region electrode and potential barrier effects have not yet begun to dominate charge transport through the device. In the high field region (>100 V), the slope of the graph m is found to lie in 1.12−1.39, indicating a nonohmic conducting mechanism.

In the high field region several possible transport phenomena in plasma polymer thin films have been reported that can be used to model the observed data.[39] The three most likely mechanisms are space-charge-limited conduction (SCLC), resistive switching (RS) conduction and Poole–Frenkel (PF) conduction. SCLC is a mechanism where the current conducted through the material is limited by a distribution of traps in the bulk material.[47] In the MIM configuration, the injection of electrons at an ohmic contact causes this space-charge-limited current.[48] RS conduction is reported in many plasma polymers, i.e., polyaniline,[49] polyfurfural,[50] and the plasma polymers of some natural extracts like lemon grass oil, eucalyptus oil, and lynalyl acetate.[47] It is a conduction mechanism where the electrons obtain enough energy to overcome the energy barrier at the metal-dielectric interface to go to the dielectric.[48] PF conduction mechanism is very similar to RS wherein the trap barrier of the material is lowered by the application of a sufficiently high electric field across the dielectric film and electrons may emit from traps into the conduction band.[47,48] The following equation is applicable to both PF and RS process:[51]

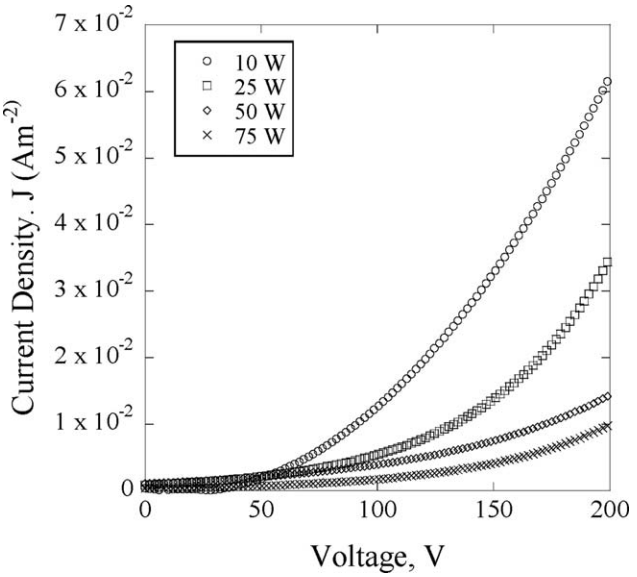

Figure 8. Current density (J) −Voltage (V) relationship for pp–GT films.

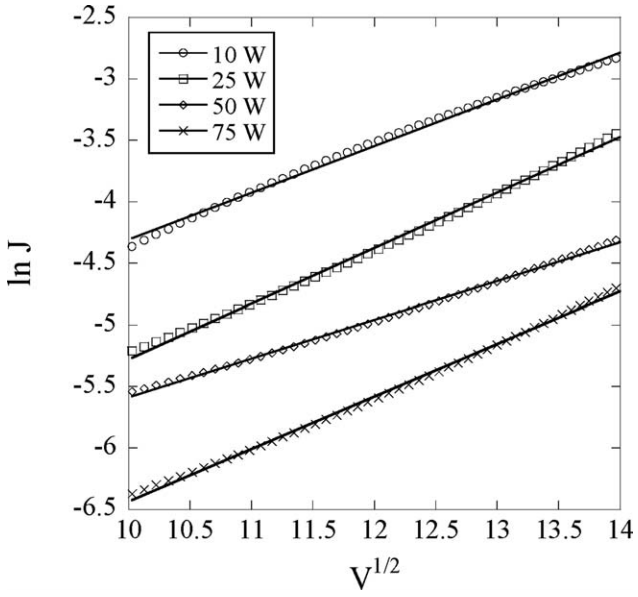

Figure 9. Variation of ln J with square root of applied voltage V for pp–GT thin films.

$$J = J_o \exp\left(\frac{\beta F^{1/2} - \phi}{kT}\right) \quad (7)$$

where J_o is the low field current density, F is the applied electric field, β is the coefficient of the static electric field, k is Boltzmann's constant in eV/K, T is the absolute temperature, and ϕ is the ionization energy of localized centers and coulomb barrier height of the electrode polymer interface in the case of PF and RS mechanisms, respectively. The parameter β is the field lowering coefficient and is given by β_{PF} and β_{RS} for PF and RS conduction, respectively:[51]

$$2\beta_{RS} = \beta_{PF} = \left(\frac{q^3}{\pi\varepsilon_0\varepsilon_r}\right)^{1/2} \quad (8)$$

where q is the charge of an electron, ε_o the permittivity of free space, ε_r the dielectric constant of the bulk material and the units of β given in eV $m^{1/2}$ $V^{-1/2}$.

In order to explain the means of conduction in insulators, each of the three aforementioned mechanisms can be used and it is important to determine which effect most adequately accounts for the charge transport. This can be achieved by analyzing the shape of the $J-V$ curves under different conditions. In the case of SCLC, double log plot of the form ln J−ln V should provide a linear characteristic, while for PF and RS conduction, plotting ln J vs. $V^{0.5}$ will provide a linear characteristic. Furthermore, differentiation between the types of the electronic conduction can be done by investigating the dependence of J on film thickness, d ($J \propto d^{-l}$) for the samples of different thickness at a constant voltage, where l is the parameter dependent on the trap distribution within the material. A slope $l < 3$ is indicative of PF or RS conduction, while $l \geq 3$ indicates the possibility of SCLC.

For pp–GT thin films, plotting ln J vs. ln V produced less linear plots than ln J vs. $V^{0.5}$ suggesting the possibility that PF or RS conduction may dominate in this region (Figure 9). Additionally, no film thickness dependence of current density was observed discounting SCLC as the dominating charge transport effect in pp–GT films. The $J-V$ characteristics in the high field region ($V > 1.5$ V) were therefore demonstrated from the viewpoint of PF and RS conduction, using eq. (8).

In order to differentiate between PF and RS mechanisms, β_{PF} and β_{RS} values can be compared with experimentally determined β coefficient (β_{exp}).[47] The following equation can be used to determine β_{exp}:

$$\beta_{exp} = skTd^{1/2} \quad (9)$$

where s is the coefficient of the linear fit of on ln J–$V^{0.5}$ characteristic. Table II summarizes the experimental and theoretical values of β calculated from eqs. (8) and (9) for pp–GT thin films.

From Table II, β_{exp} is in best agreement with β_{RS} and hence, in the higher field region Schottky mechanism is likely to dominate charge transport. Furthermore, the value of β_{exp} does not change significantly indicating that ε_r remains constant with variations in deposition power.

Electrical Resistivity Measurements. The resistivity of the pp–GT thin films was determined from the relation:

$$\rho = \frac{\left(\frac{V}{I}\right)A}{d} \quad (10)$$

where ρ is the resistivity of the material, A is the MIM structure's surface area, and d is the thin film thickness. The resistivity for

Table II. Experimental β_{exp} and Theoretical β_{PF} and β_{RS} Values of pp–GT Thin Films

RF power	β_{exp}	β_{PF}	β_{RS}
10 W	1.80×10^{-5}	4.61×10^{-5}	2.30×10^{-5}
25 W	1.82×10^{-5}	4.73×10^{-5}	2.36×10^{-5}
50 W	1.87×10^{-5}	4.79×10^{-5}	2.38×10^{-5}
75 W	1.89×10^{-5}	5.21×10^{-5}	2.60×10^{-5}

Table III. Conductivity Values (at 6 V) and Breakdown Strength (F_b) of pp–GT Thin Films

RF power	σ, S/cm	F_b, MV/cm
10 W	1.39×10^{-12}	1.48
25 W	2.91×10^{-13}	1.72
50 W	1.92×10^{-13}	1.94
75 W	1.02×10^{-13}	2.05

all pp–GT samples are in the order of 10^{10} – 10^{11} Ωm (calculated at 200 V) that confirms the insulating characteristic of pp–GT thin films. An increase in resistivity of the samples with increasing RF deposition power is attributed to the increase in degree of cross-linking in pp–GT thin films fabricated under higher powers. Furthermore, the conductivity (σ) values for films fabricated at different RF deposition powers are presented in Table III. This conductivity value is very low compared with other amorphous, plasma-deposited insulators such as plasma-polymerized thiophenes that are on the order of 10^{-6} – 10^{-10}.[50] The lowest reported conductivity for thiophenes was also found for sample fabricated at higher RF deposition powers, and this decrease attributed to the more amorphous nature of the film.

Dielectric Breakdown. Insulating properties of pp–GT thin films are determined by measuring the leakage current density with different applied fields. As the plasma power increased from 10 to 75 W, the leakage current densities decreased and the field (F_b) at which breakdown occurred, is ~2 MV/cm (Table III). This indicates that the films have a compact structure with a high density and are pinhole-free. These phenomena are well known to have a lower leakage current density and higher breakdown field. This value of 2 MV/cm is comparable to plasma deposited thiophene and octafluorocylcobutane, which have a reported value of 2 MV/cm.[40] The dielectric breakdown study was performed on pp–GT samples fabricated at 75 W, at different thicknesses (250, 500, and 800 nm) to determine whether the property showed any thickness dependence. For all the films, the breakdown field was found be ~2 MV/cm and the property of the films were therefore independent of thickness.

The dielectric strength of polymer thin films is usually dependent on various structural characteristics associated with the packing density of the materials, including the polarity, dimension, and steric structure of the molecules and/or molecular building blocks.[40] The breakdown strength (2 MV/cm) at 75 W for pp–GT film reveals that a suitable reaction environment for the γ-terpinene molecules create a relatively high concentration of small molecular activated species with mostly aliphatic C—H moieties,[33] promoting the formation of a highly cross–linked structure. The lower dielectric strengths observed for films fabricated at lower RF deposition power are attributed to the less-densely cross-linked structures.

CONCLUSIONS

Electrical properties of the plasma polymerized γ-terpinene thin films fabricated using the plasma-enhanced chemical vapor deposition is studied using the MIM structure. The real part of permittivity decreases linearly below 10 Hz for all the samples fabricated with RF powers 10, 25, 50, and 75 W. The bulk of the contribution is electronic. The initial drop in dielectric constant at low frequencies can primarily be attributed to some orientational polarization caused by the presence of trapped free radicals or the formation of polar/oxygenated groups. At a frequency of 100 KHz, the dielectric constant of samples fabricated using 10 W RF power is around 12% higher than samples fabricated using 75 W RF deposition power. The conduction mechanism responsible for the charge transport through the material was recognized as ohmic in the low voltage region, while Schottky conduction was found to be the dominating mechanism for charge transport through the films at the higher voltage region. Variations in RF deposition power did not influence the conduction mechanism, while conductivity values was found to decrease with increasing RF deposition power.

The pp–GT film cross-link density is found to play a key role in determining the breakdown strength. The continuity of the path provided to charge carriers is disrupted by increased cross-link density (as RF deposition power increases) that in turn results in higher breakdown strength. The breakdown field for the samples were in the range of 1.5 MV/cm to 2 MV/cm. No relaxation peaks were observed in the measured frequency range at room temperatures, indicative of very long relaxation times, which provide further evidence of the minimal contribution of orientation polarization to the measured relative permittivity. The dielectric function has been measured as a function of temperature, and a single relaxation peak was found to dominate the dielectric function. Determination of the distribution of relaxation times from the data using regularization methods revealed the presence of several underlying relaxation processes in addition to the dominant peak.

In summary, permittivity values of pp–GT thin films combined with high resistivity confirms the material's potential as an insulating layer for fabrication of organic electronic devices. These properties, in addition to the other desirable properties of the films such as optical transparency and high adhesion to a variety of substrates, also make pp–GT thin films a suitable candidate for other dielectric applications in electronics.

ACKNOWLEDGMENTS

J.A. is grateful to the financial support provided by the JCUPRS scholarship, and to Dr. Liam Anderson for the helpful discussions. K.B. acknowledges funding from JCU and ARC (DE130101550).

REFERENCES

1. Pai, D. Z.; Ostrikov, K.; Kumar, S.; Lacoste, D. A.; Levchenko, I.; Laux, C. O. *Sci. Rep.* **2013**, *3*.
2. Ahmad, J.; Bazaka, K.; Jacob, M. *Electronics* **2014**, *3*, 266.
3. Bazaka, K.; Jacob, M.; Truong, V.; Wang, F.; Pushpamali, W.; Wang, J.; Ellis, A.; Berndt, C.; Crawford, R.; Ivanova, E. *Biomacromolecules* **2010**, *11*, 2016.
4. Yasuda, H. Plasma Polymerisation, Academic Press: Orlando, **1985**.

5. Anderson, L. J.; Jacob, M. V. *Appl. Surf. Sci.* **2010**, *256*, 3293.
6. Bazaka, K.; Jacob, M. V. *Polym. Degrad. Stab.* **2010**, *95*, 1123.
7. Jacob, M. V.; Bazaka, K.; Weis, M.; Taguchi, D.; Manaka, T.; Iwamoto, M. *Thin Solid Films* **2010**, *518*, 6123.
8. Trabzon, L.; Awadelkarim, O. O. *Microelectron. Eng.* **2003**, *65*, 463.
9. Taur, Y.; Mii, Y. J.; Frank, D. J.; Wong, H. S.; Buchanan, D. A.; Wind, S. J.; Rishton, S. A.; Sai-Halasz, G. A.; Nowak, E. J. *IBM J. Res. Dev.* **1995**, *39*, 245.
10. Quan, Y. C.; Joo, J.; Jung, D. *Jap. J. Appl. Phys. Part 1: Regular Papers Short Notes Review Papers,* **1999**, *38*, 1356.
11. Ahmad, J.; Bazaka, K.; Anderson, L. J.; White, R. D.; Jacob, M. V. *Renewable Sustainable Energy Rev.* **2013**, *27*, 104.
12. Easton, C. D.; Jacob, M. V. *Thin Solid Films* **2009**, *517*, 4402.
13. Jiang, X.; Burgoyne, W. F. Jr; Robeson, L. M. *Polymer* **2006**, *47*, 4124.
14. Yoon, W.-J.; Bhattacharyya, D.; Timmons, R. B.; Berger, P. R. *Organ. Electron.* **2010**, *11*, 1767.
15. Biederman, H.; Slavinska, D. *Surf. Coat. Technol.* **2000**, *125*, 371.
16. Sakthi Kumar, D.; Yoshida, Y. *Surf. Coat. Technol.* **2003**, *169–170*, 600.
17. Xueqiang, L.; Weihong, B.; Tong, Z. *J. Semiconductors* **2010**, *31*, 124007.
18. Trabzon, L.; Awadelkarim, O. O.; Werking, J. *Solid-State Electron.* **1998**, *42*, 2031.
19. Biloiu, C.; Biloiu, L. A.; Sakai, Y.; Sugawara, H.; Ohta, A. *J. Vacuum Sci. Technol. A: Vacuum Surf. Films* **2004**, *22*, 1158.
20. Spanggaard, H.; Krebs, F. C. *Solar Energy Mater. Solar Cells* **2004**, *83*, 125.
21. Tai, C.-K.; Hsieh, C.-A.; Hsiao, K.-L.; Wang, B.-C.; Wei, Y. *Organ. Electron.* **2015**, *16*, 54.
22. Krebs, F. C. *Refocus* **2005**, *6*, 38.
23. Weerasinghe, H. C.; Watkins, S. E.; Duffy, N.; Jones, D. J.; Scully, A. D. *Solar Energy Mater. Solar Cells* **2015**, *132*, 485.
24. Choi, D.-W.; Kim, S.-J.; Lee, J. H.; Chung, K.-B.; Park, J.-S. *Curr. Appl. Phys.* **2012**, *12*, S19.
25. Seo, S.-W.; Jung, E.; Chae, H.; Cho, S. M. *Organ. Electron.* **2012**, *13*, 2436.
26. Kim, N.; Potscavage, Jr, W. J.; Sundaramoothi, A.; Henderson, C.; Kippelen, B.; Graham, S. *Solar Energy Mater. Solar Cells* **2012**, *101*, 140.
27. Clark, M. D.; Jespersen, M. L.; Patel, R. J.; Leever, B. J. *Organ. Electron.* **2014**, *15*, 1.
28. Jin, J.; Chen, S.; Zhang, J. *J. Polym. Res.* **2010**, *17*, 827.
29. Ma, W.; Yang, C.; Gong, X.; Lee, K.; Heeger, A. J. *Adv. Funct. Mater.* **2005**, *15*, 1617.
30. Kim, H.-K.; Kim, D. G.; Lee, K. S.; Huh, M. S.; Jeong, S. H.; Kim, K. I.; Seong, T.-Y. *Appl. Phys. Lett.* **2005**, *86*, 183503.
31. Bazaka, K.; Jacob, M. V.; Taguchi, D.; Manaka, T.; Iwamoto, M. *Chem. Phys. Lett.* **2011**, *503*, 105.
32. Anderson, L. J.; Jacob, M. V. *Thin Solid Films* **2013**, *5347*, 452.
33. Ahmad, J.; Bazaka, K.; Oelgemöller, M.; Jacob, M. V. *Coatings* **2014**, *4*, 527.
34. Jacob, M. V.; Easton, C. D.; Woods, G. S.; Berndt, C. C. *Thin Solid Films* **2008**, *516*, 3884.
35. Zong, L.; Zhou, S.; Sun, R.; Kempel, L. C.; Hawley, M. C. *J. Polym. Sci. B: Polym. Phys.* **2004**, *42*, 2871.
36. Casalini, R.; Fioretto, D.; Livi, A.; Lucchesi, M.; Rolla, P. A. *Phys. Rev. B* **1997**, *56*, 3016.
37. Corrales, T.; Villavieja, M. M.; Peinado, C.; Bosch, P. *J. Photochem. Photobiol. A: Chem.* **2006**, *182*, 52.
38. Endo, K.; Shinoda, K.; Tatsumi, T. *J. Appl. Phys.* **1999**, *86*, 2739.
39. Dakhel, A. A. *J. Non-Crystalline Solids* **2007**, *353*, 1529.
40. Jiang, H.; Hong, L.; Venkatasubramanian, N.; Grant, J. T.; Eyink, K.; Wiacek, K.; Fries-Carr, S.; Enlow, J.; Bunning, T. J. *Thin Solid Films* **2007**, *515*, 3513.
41. Goswami, A.; Goswami, A. P. *Thin Solid Films* **1973**, *16*, 175.
42. Phadke, S. D. *Thin Solid Films* **1978**, *48*, 319.
43. Prins, P.; Grozema, F. C.; Schins, J. M.; Siebbeles, L. D. A. *physica status solidi (b)* **2006**, *243*, 382.
44. Singha, S.; Thomas, J. M. *IEEE Transact. Dielectrics Electrical Insulat.* **2008**, *15*, 2.
45. El-Shabasy, M.; Riad, A. S. *Physica B: Condensed Matter* **1996**, *222*, 153.
46. Seyam, M. A. M. *Appl. Surf. Sci.* **2001**, *181*, 128.
47. Anderson, L. J.; Jacob, M. V. *Mater. Sci. Eng. B* **2012**, *177*, 311.
48. Chiu, F.-C. *Adv. Mater. Sci. Eng.* **2014**, *2014*, 18.
49. Mathai, C. J.; Saravanan, S.; Jayalekshmi, S.; Venkitachalam, S.; Anantharaman, M. R. *Mater. Lett.* **2003**, *57*, 2253.
50. Silverstein, M. S.; Visoly-Fisher, I. *Polymer* **2002**, *43*, 11.
51. Majumder, S.; Bhuiyan, A. H. *Polym. Sci. Series A* **2011**, *53*, 85.